

COUPLED DEM-CFD APPROACH TO MODELLING NON-SPHERICAL PARTICLE SEDIMENTATION IN 3D

Gary W. DELANEY¹, James E. HILTON¹, Paul W. CLEARY¹ and Claire MILLER¹

¹ CSIRO Mathematics, Informatics and Statistics, Clayton, Victoria 3169, AUSTRALIA

ABSTRACT

We investigate a common industrial sedimentation case where an insoluble solid is separated from a liquid in which it was initially suspended by settling under the influence of gravity. We employ a coupled DEM-CFD approach to model the sedimentation of non-spherical particles in 3D. Our simulations are performed in a tall rectangular box, with a fixed base and periodic boundary conditions at the sides. The particles are modelled as ellipsoids and the fluid is simulated as a Stokesian liquid. The effects of particle shape, viscosity and inter-grain friction are studied and related to the structure of the final packed bed that is formed by the sedimenting particles. We find that the lowest bulk densities are achieved for systems of particles with high inter-particle friction, sedimented in a highly viscous fluid. Order parameters are used to characterise the structure of the final packed beds. Significant orientational ordering of the grains is found to occur, particularly for particles with higher aspect ratios. The consequences of the results for established definitions of different states of granular matter are discussed.

NOMENCLATURE

A	particle area of volume equivalent sphere
A'	particle area of projected in flow direction
C_n	particle normal damping coefficient
C_t	particle tangential damping coefficient
\mathbf{f}_d	fluid body force
\mathbf{F}_b	particle buoyancy force
\mathbf{F}_c	particle contact force
\mathbf{F}_d	particle drag force
\mathbf{g}	gravitational acceleration
k_n	particle normal spring stiffness
k_t	particle tangential spring stiffness
m	particle mass
p	fluid pressure
\mathbf{T}_D	drag torque
\mathbf{u}	fluid velocity
\mathbf{u}_r	relative fluid-particle velocity
\mathbf{v}	particle velocity
V	particle volume
χ_θ	orientational order parameter
η	fluid dynamic viscosity
ρ_f	fluid density
μ	particle friction coefficient
Φ	packing fraction
ϕ	particle sphericity
ϕ'	particle crosswise sphericity
$\boldsymbol{\omega}_p$	particle spin vector
$\boldsymbol{\omega}_r$	relative spin vector

INTRODUCTION

In an industrial context, sedimentation refers to the separating out of solid particles from a liquid in which they are suspended. The driving mechanism for this separation is a force applied to the particles, which may be due to centrifugal acceleration, electromagnetism, or most commonly, gravity. Sedimentation processes are very important in a broad range of industrial activities, including in water treatment processes, where suspended particles, such as clay or silts, present in the source water are removed (Raudkivi 1993).

When a set of spherical grains is allowed to settle into a packed state, a random packing will generally be formed, with the density of the final assembly lying between what are referred to as the “random loose packing” (RLP) and “random close packing” (RCP) limits. These two limits have been extensively studied, but establishing their strict definitions has been a challenge. This is in large part due to the competition between order and density, which allows one to generate increasingly dense packings at the expense of increasing the order within the system. For dense packings, the maximally random jammed state has been proposed as a means of resolving these two competing effects, and has a precise definition for frictionless hard particles as the jammed packing that minimizes a chosen order parameter (Torquato, Truskett, and Debenedetti 2000).

Sedimentation techniques have long been employed in the study of granular materials as a controlled protocol for generating packed granular systems at a range of densities (Scott and Kilgour 1969). Until recently these investigations centred on the study of spherical grains. Sedimentation techniques are particularly useful for studying loose packings. For spheres, a lower limit on the packing fraction of $\Phi \approx 0.55$ is achieved for particles with a high inter-grain friction, sedimented slowly in a viscous fluid (Onoda and Liniger 1990; Jerkins et al. 2008). For spheres, this results in a packing that is essentially random, with a range of order parameters suggesting very little ordered structure exists within the packings generated by spheres using this technique.

We consider the case of a set of non-cohesive ellipsoidal particles that settle in a viscous fluid. Our primary focus in this paper will be considering the effect of particle shape, inter-grain friction and fluid viscosity on the properties of the final packed bed that is created from the sedimentation process. In our previous work considering sedimentation of monodisperse systems of prolate ellipsoids (Delaney et al. 2011), we demonstrated the important effect of particle shape in determining the structural properties of packings of prolate ellipsoids generated by sedimentation techniques. (A prolate ellipsoid is one in which the particle has two shorter axes

of equal length and one longer major axis.) We found that while a loose limit was obtained for particles with high inter-grain friction sedimented in a viscous fluid, the packings were not random, with the grains exhibiting a high degree of orientational ordering of their major axes. These results demonstrated that the previously accepted definition of random loose packing in terms of the loosest packing that could be obtained by pouring (or sedimenting) grains was not suitable for particle shapes beyond perfect spheres.

In this paper, we will consider the case of oblate ellipsoids, where the ellipsoids have two longer axes of equal length and one shorter axis. We will also consider mixtures of equal numbers of prolate and oblate ellipsoids, and bidisperse packings of oblate ellipsoids with different volume ratios. We will investigate the extent to which these grain shapes and sizes affect the density and the structural properties of the packings generated using sedimentation techniques.

MODEL DESCRIPTION

Particles in the simulation are modelled using the Discrete Element Method (DEM), in which the forces and torques on each particle are individually time-integrated to give the positions and velocities of the particles at subsequent time steps (Cundall and Strack 1979) (Cleary 2004). The equation of motion for a single particle is given by:

$$m \frac{\partial \mathbf{v}}{\partial t} = \mathbf{F}_c + \mathbf{F}_d + \mathbf{F}_b + m\mathbf{g} \quad (1)$$

where m is the particle mass, \mathbf{v} the particle velocity, \mathbf{F}_c the collisional forces, \mathbf{F}_d the drag force, \mathbf{F}_b the buoyancy force on the particle, and \mathbf{g} the gravitational acceleration. The collisional force, \mathbf{F}_c , is composed of the normal collisional force, \mathbf{F}_n , and the tangential collisional force, \mathbf{F}_t , acting on the particle, $\mathbf{F}_c = \mathbf{F}_n + \mathbf{F}_t$, which act along the normal and in the tangent plane at the contact point, respectively. The magnitude of the normal force is calculated from a linear-spring dashpot model:

$$F_n = C_n v_n - k_n \delta l \quad (2)$$

where k_n is a spring stiffness, chosen to ensure the overlap, δl , between contacting particles does not exceed $\sim 0.1\%$ of the particle diameter, on average. The normal damping coefficient C_n gives the required coefficient of restitution, and v_n is the relative normal speed. The magnitude of the tangential force is incrementally calculated from:

$$F_t = \min \left\{ \begin{array}{l} \mu F_n \\ C_t v_t + k_t \sum v_t \Delta t \end{array} \right\} \quad (3)$$

where μ is the Coulomb coefficient of friction, k_t a tangential spring stiffness, v_t the relative tangential velocity, Δt the time-step and C_t a tangential damping coefficient. The incremental sum in this expression applies over the duration of the contact, and models the tangential elastic deformation of the surface. The incremental sum and dashpot is limited by the Coulomb friction μF_n .

The fluid is modelled using the constitutive relations for a highly viscous, Stokesian, fluid:

$$\rho_f \frac{\partial \mathbf{u}}{\partial t} = -\nabla p + \eta \nabla^2 \mathbf{u} + \mathbf{f}_d \quad (4)$$

$$\nabla \cdot \mathbf{u} = 0$$

where ρ_f is the fluid density, \mathbf{u} the velocity, p the pressure, η the viscosity and \mathbf{f}_d the fluid body drag forces. These are the usual Navier-Stokes relations without the term involving convective acceleration. This term is neglected in a Stokesian fluid as the assumption is made that the Reynolds number, Re , is much smaller than unity, as the fluid is dominated by viscous forces.

The Stokesian fluid is modelled using Eq. (4), discretised over a regular Cartesian grid (Delaney et al. 2011). A pressure correction method is used where, as a first step, the pressure gradient term is neglected and the parabolic relation involving the Laplacian term is solved using a Crank-Nicolson algorithm. Next, a pressure correction is calculated to enforce the divergence free condition of the fluid. A second order Runge-Kutta method (Heun's method) is used to integrate forward in time. The method is based on an unresolved particle-fluid coupling method for fluid flow through particle beds (Hilton et al. 2010). Unresolved methods model the particles as a volume averaged porous medium within each cell, requiring that the largest particles in the simulation must fit entirely within a cell. Such volume averaging is used in this case as the fine scale dynamics of Stokesian flow around the particle are not required. In this application the fluid serves only to affect the particle through viscous drag, allowing it to slowly settle on the particle bed.

Accurate coupling between the fluid and particles is essential for particle-fluid systems. Here, we use the following fluid-particle drag force:

$$\mathbf{F}_d = \frac{1}{2} C_d A' \rho_f |\mathbf{u}_r|^2 \hat{\mathbf{u}}_r$$

$$\mathbf{f}_d = \sum_{i=0}^N \mathbf{F}_d^i \quad (5)$$

where C_d is a non-spherical drag coefficient, which applies over all Reynolds numbers, A' is the area of the particle projected in the flow direction and \mathbf{u}_r is the relative fluid-particle flow velocity, $\mathbf{u}_r = \mathbf{u} - \mathbf{v}$. The summation for the body force term is taken over all N particles in the computational cell volume. The non-spherical drag coefficient is taken from an empirical formula given by Hölzer and Sommerfeld (2008):

$$C_d = \frac{8}{Re} \left(\frac{1}{\sqrt{\varphi'}} + \frac{2}{\sqrt{\varphi}} \right) + \frac{3}{\sqrt{\varphi^{0.75}}} + \frac{0.42}{\varphi'} 10^{0.4(-\log \Phi)^{0.2}} \quad (6)$$

where the regular sphericity, Φ , is the ratio between the surface area of the volume equivalent sphere and the surface area of the considered particle. The crosswise sphericity, φ' , is the ratio between the cross-sectional area of the volume equivalent sphere, A , and the projected cross-sectional area of the considered particle perpendicular to the flow, A' , so $\varphi' = A/A'$. The area A' is calculated using numerical integration of the area with the projected rim of the non-spherical particle onto the plane orthogonal to the flow direction (Hilton et al. 2010). The Hölzer and Sommerfeld drag relation gives a good match to experiments carried out over a wide range of particle shapes, and is used here as implicitly contains area dependant terms, which are especially important for ellipsoids.

The particles also experience a rotational drag torque given by:

$$\mathbf{T}_D = 8\pi\eta r^3 \boldsymbol{\omega}_r \quad (7)$$

where $\boldsymbol{\omega}_r$ is a relative spin vector given by $\boldsymbol{\omega}_r = \frac{1}{2} \nabla \times \mathbf{u} - \boldsymbol{\omega}_p$, where $\boldsymbol{\omega}_p$ is the particle spin vector. It should be noted that the particle-fluid model is unresolved, so no torque dependency on the orientation angle can be included in this expression as the pressure distribution over the computational cell is volume averaged. A buoyancy force is also incorporated into the model, given by:

$$\mathbf{F}_b = \rho_f V \mathbf{g} \quad (8)$$

where V is the volume of the particle.

SIMULATION SETUP

The simulation setup is shown in **Figure 1**. The simulation box is rectangular with a fixed base and periodic boundary conditions at each side. The box has a height of 0.8 m, and a square cross-section of width 0.1 m. Particles were initially distributed with random coordinates and orientations within the box. The base of the simulation box has a layer of ellipsoids fixed in position at random orientations, so as to ensure that the grains are settling onto a disordered surface, which ensures that no ordering effects are caused by particles simply aligning on a flat base.

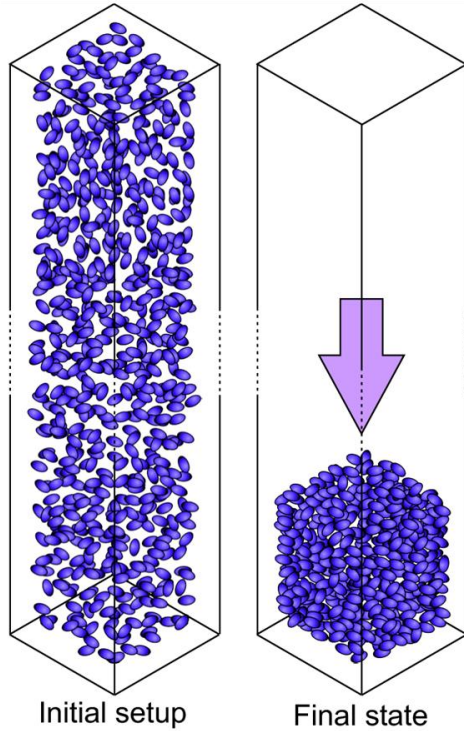


Figure 1: Illustration showing the initial and final states for the particles in the simulation.

Particles simulated were either prolate or oblate ellipsoids defined by:

$$\frac{x^2}{a^2} + \frac{y^2}{b^2} + \frac{z^2}{c^2} = 1$$

For all the simulations considered in this paper, two axes a and b have equal length, and the length of the third axis c was varied to generate ellipsoids with different aspect ratios. The aspect ratio α is then given by the ratio of the shortest axis length to the longest axis length for the

ellipsoid. Prolate ellipsoids have two equal shorter axes, while oblate ellipsoids have two equal longer axes.

Quantification of orientational ordering

We examine the ordering present in the packings by quantifying the degree of orientational alignment of the grains. Our previous work (Delaney, et al., 2011), considering frictional packings of mono-disperse prolate ellipsoids, demonstrated the presence of considerable orientational ordering of the grains, with the grains major axes preferentially aligning in the plane normal to the vertical direction. Similar results have also been found for frictionless packings of ellipsoids generated using Monte Carlo techniques (Buchalter and Bradley 1994). The presence of this type of ordering can easily be understood. The lowest energy position for a prolate ellipsoid placed on a surface under the influence of gravity is for its centre of mass to be at the lowest possible height. This will correspond to its semi-major axis lying flat in the plane normal to the vertical direction. For an oblate ellipsoid, by the same argument, its lowest energy position will correspond to its semi-minor axis pointing in the vertical direction, with its two longer axes lying flat in the plane normal to the vertical.

We quantify the degree of orientational alignment using appropriate order parameters for prolate and oblate ellipsoids respectively (Delaney, Hilton, and Cleary 2011). For prolate ellipsoids this order parameter is given by:

$$\chi_\theta = \frac{3}{2} \left\{ \frac{1}{N} \sum_{i=1}^N \cos 2 \left(\theta_i - \frac{\pi}{2} \right) - \frac{1}{3} \right\}$$

where θ_i is the angle between the semi-major axis of the i^{th} ellipsoid and the vertical axis. The order parameter for the oblate grains is given by:

$$\chi_\theta = \frac{3}{4} \left\{ \frac{1}{N} \sum_{i=1}^N \cos(2\theta_i) + \frac{1}{3} \right\}.$$

These measures are chosen so that if all particles within a packing were randomly orientated, then the order parameters would be 0. If all particles lie flat with their major axes oriented in the plane normal to the vertical, then the order parameter would be 1.

RESULTS

Mono-disperse packings of oblate ellipsoids

Figure 2 shows the packing fraction variation with aspect ratio for systems of mono-disperse oblate ellipsoids. Two cases are shown, which correspond to the extreme cases of a) inter-grain friction ($\mu = 0$) without a background fluid ($\eta = 0$), and b) high inter-grain friction ($\mu = 1000$) and high viscosity ($\eta = 1.0$ Pa s). The value of $\mu = 1000$ is chosen so that we are essentially in the infinite friction limit (Delaney, 2011). These two cases produce packings close to the densest and loosest limits that can be obtained through the sedimentation technique employed.

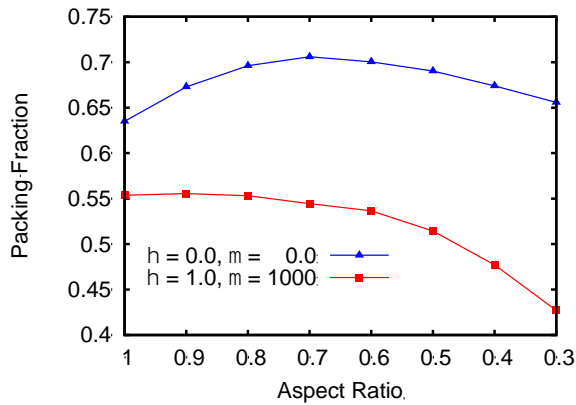


Figure 2: Packing fraction variation with aspect ratio for mono-disperse packings of oblate ellipsoids. Data is shown for the two extreme cases of zero inter-grain friction without a background fluid (blue triangles) and high inter-grain friction and high viscosity (red squares).

For dense packings created with zero inter-grain friction and zero fluid viscosity, the packing fraction for spheres ($\alpha = 1.0$) is close to the random close packing limit (RCP) value of $\Phi \approx 0.64$. As the aspect ratio is varied from unity, we obtain a peak in packing fraction at

an aspect ratio of around 0.7 followed by a near linear decline. These results are similar to those seen for prolate ellipsoids packings prepared by the same technique (Delaney, et al. 2011) and also for random close packings of ellipsoids prepared by a particle expansion technique (Delaney and Cleary 2010).

For the loose packings prepared with high inter-particle friction ($\mu = 1000$) in a high viscosity fluid ($\eta = 1.0$ Pa s), we obtain packing fractions similar to those measured for the random loose packing limit for spheres at $\Phi \approx 0.55$. As the aspect ratio is varied from unity, we see an initial plateau and then a steady decline between 0.8 and 0.6 followed by a faster rate of decrease. This variation in packing fraction for oblate ellipsoids, is again similar to that observed for prolate ellipsoids by (Delaney, et al., 2011).

Figure 3 shows images of packings of mono-disperse oblate ellipsoids with the particles coloured by the degree of alignment with the horizontal axis. The strong orientational alignment of the ellipsoids with the horizontal axis for the dense packings (Figure 3a) created with zero inter-grain friction can clearly be seen by the large fraction of ellipsoids coloured red in the image. Conversely the lower degree of orientational ordering can be seen for the loose packing (Figure 3b) by the greater number of grains coloured blue that are not orientated in

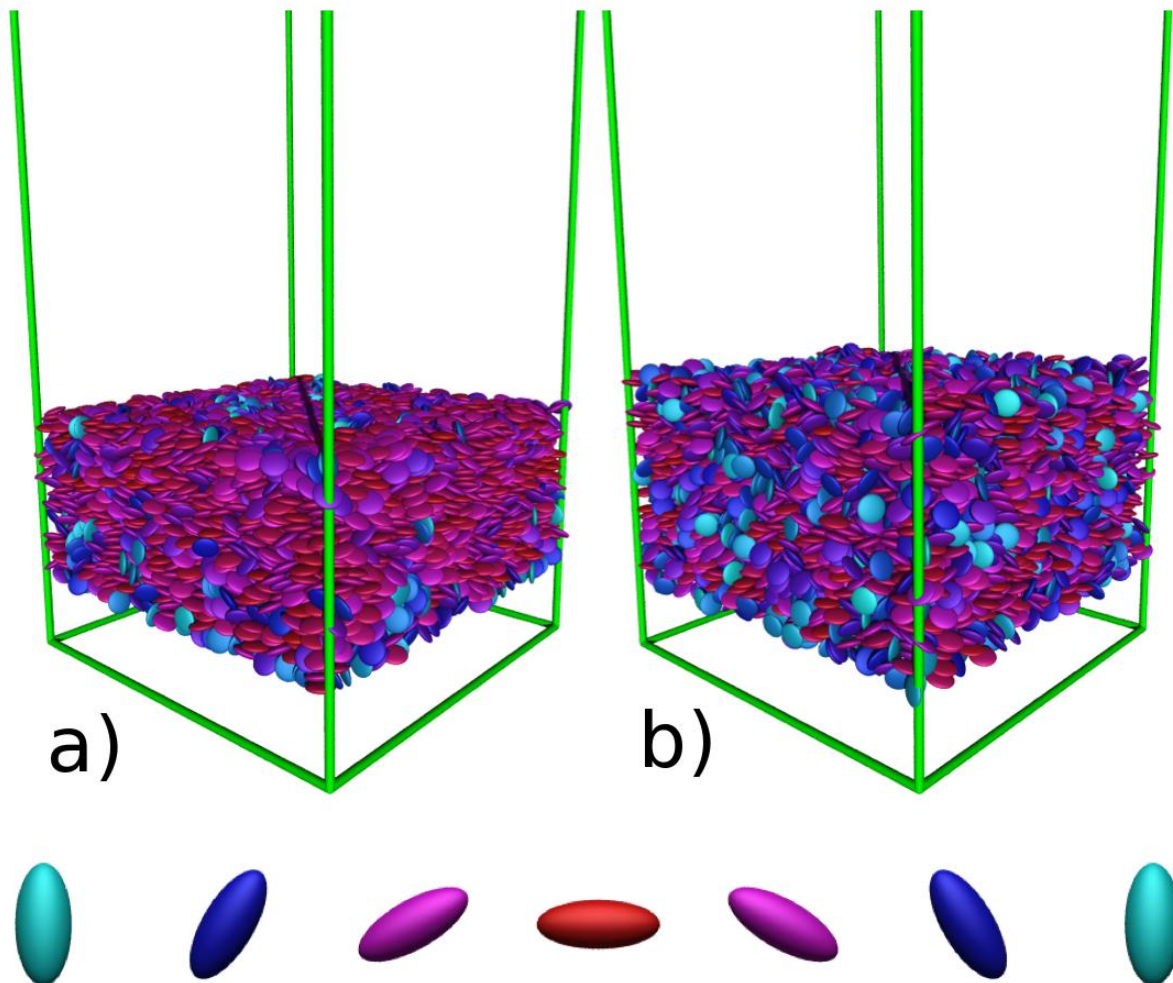


Figure 3: Images of packings of monodisperse oblate ellipsoids with an aspect ratio of 0.3 at the a) dense, and b) loose limits. Particles are coloured by the alignment of the grain with the horizontal axis as shown in the key.

the horizontal direction.

The corresponding variation in the orientational order parameter χ_θ for mono-disperse packings of oblate ellipsoids is shown in Figure 4. For both the dense ($\eta = 0$ Pa s, $\mu = 0$) and loose ($\eta = 1.0$ Pa s, $\mu = 1000$) packings, there is a monotonic increase in the degree of orientational ordering as the aspect ratio is varied. The degree of ordering at each aspect ratio is consistently higher for the dense packings compared to the loose packings. The difference between the degree of ordering observed for the dense and loose packings increases as the aspect ratio becomes more extreme, with the largest difference being for $\alpha = 0.3$.

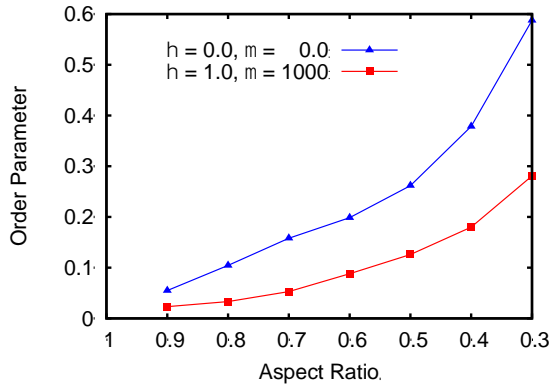


Figure 4: Orientational order parameter χ_θ for mono-disperse packings of oblate ellipsoids. Data is shown for the two extreme cases of zero inter-grain friction without a background fluid (blue triangles) and high inter-grain friction and high viscosity (red squares).

For the dense packings there is no direct correlation between ordering and density, with a consistent monotonic increase in ordering with aspect ratio, in contrast to the peak in density found at an aspect ratio around 0.7. For the loose packings, there is an inverse correlation between order and density at high aspect ratios. This could suggest that the orientational alignment of the grains at high aspect ratios is a contributing factor in the low packing densities achieved for the high aspect ratio grains with high inter-grain friction.

Mixtures of equal volume prolate and oblate ellipsoids

We now consider packings formed by 50:50 mixtures of equal volume prolate and oblate ellipsoids with the same aspect ratio α . The initial setup for these simulations has equal numbers of prolate and oblate ellipsoids placed at random positions within the simulation box.

Figure 5 shows the packing fraction variation for the extreme cases of a) dense packings formed using zero inter-grain friction ($\mu = 0$) without a background fluid ($\eta = 0$), and b) loose packings formed using high inter-grain friction ($\mu = 1000$) and high viscosity ($\eta = 1.0$ Pa s). The packing fractions are quiet close to those observed for mono-disperse packings in Figure 2. The largest differences are seen for aspect ratios far from unity for the loose packings, where packing fractions approximately 2% below those of the mono-disperse oblate packings are observed.

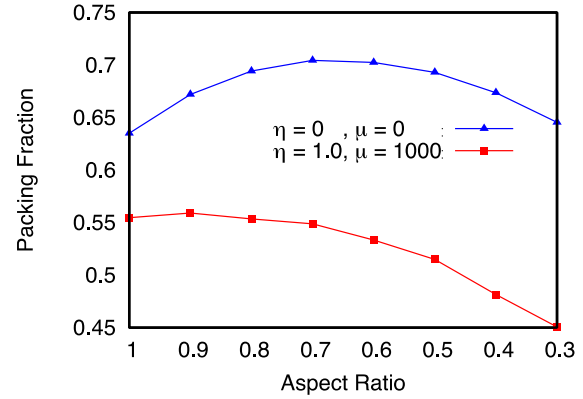


Figure 5: Packing fraction variation with aspect ratio for 50:50 mixtures of prolate and oblate ellipsoids.

Figure 6 shows the variation in the orientational order parameter with aspect ratio for densely packed mixtures of ellipsoids. Data is shown for all ellipsoids in the packings and separately for the oblate and prolate particles. There is again a monotonic increase in orientational ordering as the aspect ratio is varied from unity, with the prolate ellipsoids in the mixtures showing consistently larger amounts of orientational ordering compared to the oblate ellipsoids.

Figure 7 shows the variation in the orientational order parameter with aspect ratio for loosely packed mixtures of ellipsoids. Again there is a monotonic increase in the orientational ordering, with the prolate ellipsoids showing a higher degree of order. The rate of increase in ordering is initially quite slow as the aspect ratio is varied away from unity, and then increases for more extreme aspect ratios.

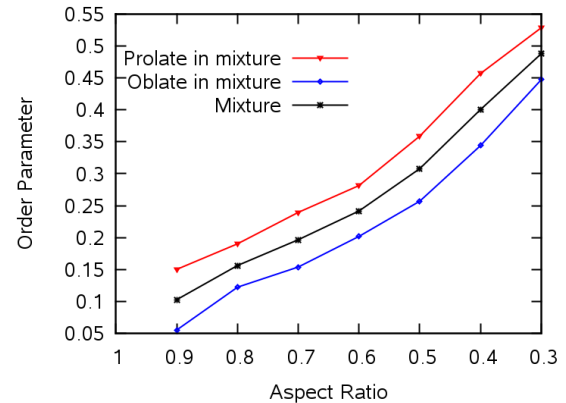


Figure 6: Variation in the orientational order parameter with aspect ratio for 50:50 mixture of oblate and prolate ellipsoids with the same aspect ratio. Packings were prepared with zero inter-grain friction without a background fluid.

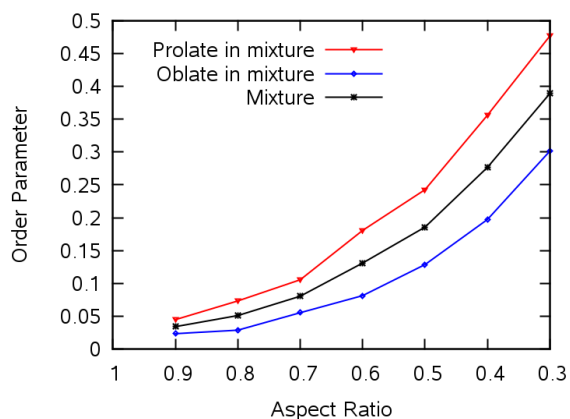


Figure 7: Variation in the orientational order parameter with aspect ratio for 50:50 mixture of oblate and prolate ellipsoids with the same aspect ratio. Packings were prepared with high inter-particle friction ($\mu = 1000$) in a high viscosity fluid ($\eta = 1.0$ Pa s).

Bi-disperse packings of oblate ellipsoids

We next consider packings of bidisperse oblate ellipsoids at a range of volume ratios. These packings are composed of 50:50 mixtures of equal numbers of two different sizes of oblate ellipsoids with the same aspect ratio. Volume ratios of 2:1, 4:1 and 6:1 were considered. These packings were generated for frictionless grains under free fall without a fluid. The larger of the two particles in each packing was kept at a fixed volume equivalent to that of a 3.175 mm radius sphere. Figure 8 shows an image of the formation of a bidisperse packing of ellipsoids with aspect ratio 0.4 and a volume ratio of 6:1.

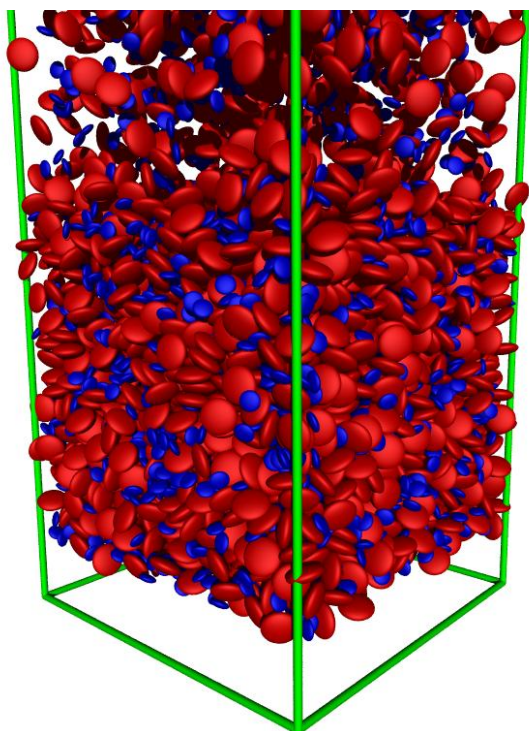


Figure 8: Image of the formation of a bi-disperse packing of oblate ellipsoids with aspect ratio of 0.4 and a volume ratio of 6:1.

Figure 9 shows the packing fraction variation with aspect ratio for bi-disperse ellipsoid packings at particle volume ratios of 2:1, 4:1 and 6:1. As the aspect ratio is varied, there is an initial increase in packing fraction, and then a fall off at aspect ratios further from unity. This is similar to the behaviour seen for mono-disperse packings. For all aspect ratios, there is a monotonic increase in the packing fraction with increasing particle volume ratio. This is due to the smaller volume ellipsoids being able to more easily fill the pores between the larger particles, leading to a denser packing being formed.

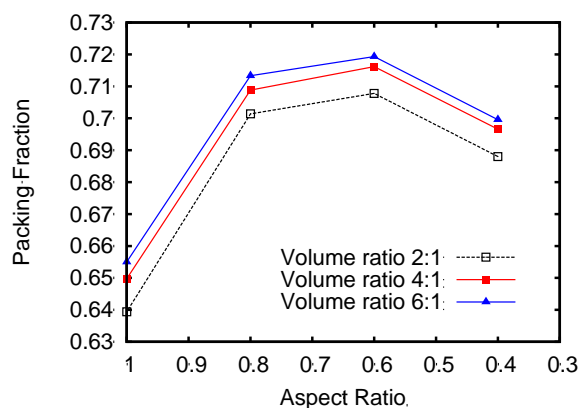


Figure 9: Packing fraction variation with aspect ratio for dense bi-disperse packings of oblate ellipsoids. Three particle volume ratios are shown. Packings were created with zero inter-grain friction and without a background fluid.

Figure 10 shows the variation in the orientational order parameter with aspect ratio for bi-disperse ellipsoid packings at a range of aspect ratios. For all particle volume ratios there is a monotonic increase in the orientational ordering as the aspect ratio is increased. There is a decrease in the orientational ordering of the ellipsoids at a given aspect ratio as the volume ratio is increased.

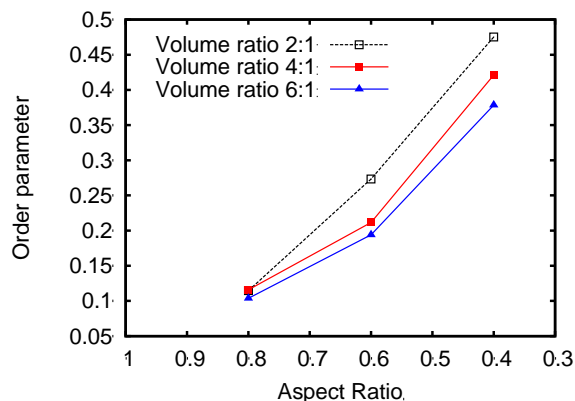


Figure 10: Variation in the orientational order parameter with aspect ratio for bi-disperse packings of ellipsoids.

The increase in the size difference results in a higher density, less ordered packing. The higher density is attributable to the size difference between the particles making it possible for the smaller particles to fit in the gaps between the larger particles. We have also individually determined the orientational ordering for each of the sizes within the packings, and have found that the smaller particles have a lower tendency to order than the

larger ones. This may be due to the smaller particles having a tendency to become trapped in the irregular pores formed by the larger particles, and not being able to slide into an orientation with their semi-minor axes aligned with the vertical direction.

CONCLUSION

Our results demonstrate the important effect of particle shape in determining the final structural properties of packed granular systems formed via sedimentation processes. Across all the systems considered, we have found that increasing aspect ratio leads to increased orientational alignment of the grains. This is due to the greater potential energy penalty that is incurred for the grains to not lie flat with their major axes lying in the plane normal to gravity. Results for mixtures of prolate and oblate ellipsoids, showed a greater degree of orientational alignment of prolate over oblate ellipsoids. Our consideration of bidisperse packings of oblate ellipsoids, showed an increase in packing density as we increased the size difference between the two species up to a volume ratio of 6:1. We also found a decrease in the overall orientational ordering within the system as the volume ratio was increased.

In (Delaney et al. 2011), we presented results for monodisperse packings of prolate ellipsoids and demonstrated that the previously accepted definition of random loose packing in terms of the loosest packing that could be obtained by pouring (or sedimenting) grains, was not suitable for particle shapes beyond perfect spheres. The results presented here demonstrate that such a definition is also inapplicable to a broader range of particle shapes and to mixtures of shapes and bidisperse systems. This highlights the need for new and better definitions to characterise the different states of packed granular matter.

REFERENCES

BUCHALTER, B. J., and R. M. BRADLEY. (1994). "Orientational Order in Amorphous Packings of Ellipsoids." *EPL (Europhysics Letters)* 26 (3): 159–164.

CLEARY, PAUL W. 2004. "Large Scale Industrial DEM Modelling." *Engineering Computations* 21 (2/3/4): 169 – 204.

CUNDALL, PA, and ODL STRACK. (1979). "A Discrete Numerical Model for Granular Assemblies." *Geotechnique* 29 (1): 65, 47.

DELANEY, G. W., and P. W. CLEARY. (2010). "The Packing Properties of Superellipsoids." *EPL (Europhysics Letters)* 89 (3) : 34002.

DELANEY, GARY W., JAMES E. HILTON, and PAUL W. CLEARY. 2011. "Defining Random Loose Packing for Nonspherical Grains." *Physical Review E* 83 (5) : 051305.

HILTON, J.E., MASON, L.R. and CLEARY, P.W., 2010. "Dynamics of gas-solid fluidised beds with non-spherical particle geometry", *Chem. Eng. Sci.*, 65, 1584-1596

JERKINS, MELISSA, MATTHIAS SCHROTER, HARRY L. SWINNEY, TIM J. SENDEN, MOHAMMAD SAADATFAR, and TOMASO ASTE.

(2008). "Onset of Mechanical Stability in Random Packings of Frictional Spheres." *Physical Review Letters* 101 (1) : 018301–4.

ONODA, GEORGE Y., and ERIC G. LINIGER. (1990). "Random Loose Packings of Uniform Spheres and the Dilatancy Onset." *Physical Review Letters* 64 (22) : 2727.

RAUDKIVI, ARVED J. (1993). *Sedimentation: Exclusion and Removal of Sediment from Diverted Water*. Taylor & Francis.

SCOTT, G. D., and D. M. KILGOUR. (1969). "The Density of Random Close Packing of Spheres." *Journal of Physics D: Applied Physics* 2 (6): 863–866.

TORQUATO, S., T. M. TRUSKETT, AND P. G. DEBENEDETTI. (2000). "Is Random Close Packing of Spheres Well Defined?" *Physical Review Letters* 84 (10) : 2064.